ACS Sustainable Chemistry & Engineering

pubs.acs.org/journal/ascecg

Research Article

Introducing Protein Crystallization in Hydrated Deep Eutectic Solvents

Benny Danilo Belviso, Filippo Maria Perna, Benedetta Carrozzini, Massimo Trotta,* Vito Capriati,* and Rocco Caliandro*

Cite This: *ACS Sustainable Chem. Eng.* 2021, 9, 8435–8449

Read Online

ACCESS | Metrics & More | Article Recommendations | Supporting Information

ABSTRACT: Supramolecular structure and properties of deep eutectic solvents (DESs) are known to be highly affected by the addition of water, and their use as solvents for poorly water-soluble macromolecules is being actively investigated. We report the first experimental investigation of protein crystallization in DESs. Different hydrophilic and hydrophobic eutectic mixtures, hydrated at different levels, have been screened as crystallization media. DESs were added to the solution containing the precipitant and the buffer required to crystallize three test proteins, and we observed that the volume ratio between DES and the corresponding solution is a key parameter for the crystallization process. Successful crystallization was achieved for the hen-egg white lysozyme when using choline chloride:urea, choline chloride:glycerol, and choline chloride:-glutamic acid eutectic mixtures at a 1:2 molar ratio. High-resolution X-ray diffraction experiments disclosed the possibility to study the intriguing supramolecular network of the molecular complexes formed between protein and DES in the presence of water molecules. Individual DES components have been found to systematically occupy specific protein sites populated by solvent-exposed aromatic residues. Weak interactions between DES components, possibly mediated by water molecules, which resulted in being frozen in the ordered solvent surrounding the protein units in the crystal lattice, were reconstructed at atomic resolution. DESs were found to have a negligible effect on the protein conformation and its flexibility in the solid state. On the other hand, DESs greatly reduced solvent evaporation from the crystallization drop, thereby increasing the dissolution time of the protein crystals. Finally, DESs were found to serve as local modulators of the ordered solvent, and this resulted in a significant change of the protein solubility. In addition, we found that protein crystallization was sped up by tuning DES hydration. This enables the employment of these environmentally responsible solvents to improve biotechnological processes at the industrial level.

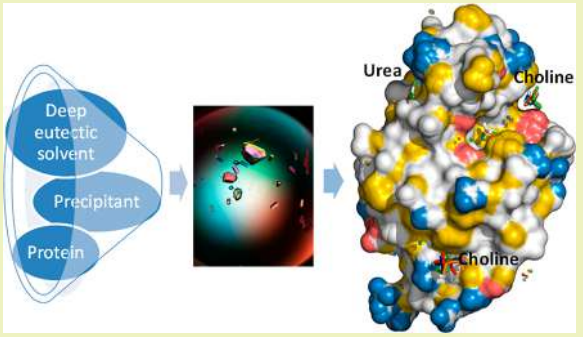

KEYWORDS: *deep eutectic solvents, lysozyme, protein crystallization, crystal structure, protein−DES interactions, crystal dissolution*

Downloaded via Vito Capriati on July 1, 2021 at 09:54:32 (UTC).
See https://pubs.acs.org/sharingguidelines for options on how to legitimately share published articles.

INTRODUCTION

Binary or ternary liquid mixtures formed by pure chemical compounds comprising at least one hydrogen bond donor (HBD) and one hydrogen bond acceptor (HBA) strongly associate with each other via hydrogen bond interactions. When mixed in a proper molar ratio, these compounds form a eutectic solution with a melting point much lower than those of the individual components and that of an ideal liquid mixture and, hence, are called deep eutectic solvents (DESs).[1−3]

Eutectic mixtures formed by natural compounds (e.g., amino acids, amino alcohols, carbohydrates, vitamins, polyalcohols) are particularly attractive from both an ecological point of view and an economic perspective as they are biodegradable, poorly toxic, and inexpensive.[4] They are progressively replacing toxic volatile organic compounds in several fields of science, like organometallics,[5,6] catalysis,[7−12] electrochemistry,[13] photosynthesis,[14] and solar technology,[15] their physicochemical properties being highly tunable.

Interestingly, as for the biocatalytic aspects, DESs have proven nondetrimental when used as solvents[16] for proteins and enzymes, maintaining the activity of macromolecules even in the case of membrane proteins[14] and sparely soluble macromolecules.[17]

Industrial biocatalytic processes highly benefit from enzyme immobilization, a strategy that enables an easy reuse of the biocatalyst and allows an easy recovery of the final product.[18] Among the current immobilization strategies, the use of enzyme crystals, suitably cross-linked or embedded into proper supports, is very attractive for biotechnological applications.[19] In addition, effective protein crystallization methods are of

Received: February 22, 2021
Revised: May 31, 2021
Published: June 15, 2021

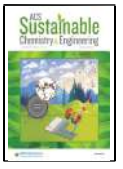

© 2021 American Chemical Society

https://doi.org/10.1021/acssuschemeng.1c01230
ACS Sustainable Chem. Eng. 2021, 9, 8435−8449

interest in structural biology, where the main bottleneck is that of obtaining well-diffracting single crystals.

Protein crystallization was found to improve by using hydrophobic membranes and hydrogel layers, called hydrogel composite membranes (HCMs).[20] While membranes control vapor diffusion and induce heterogeneous crystallization, hydrogels influence the crystal growth affecting the crystal lattice properties. In particular, the hydrogel layer preserves embedded protein crystals from osmotic stress (e.g., pH, *T*, and *P* changes, effect of radicals), thereby increasing their lifetime.[21] Moreover, HCMs enhance the enzymatic activity, hence reducing the quantity of enzyme required,[21] and promote the crystal growth,[22] accelerating the kinetics of crystal formation.

Ionic liquids (liquids composed of weakly coordinated ionic species with melting points below 100 °C) [e.g., ethylammonium nitrate, 1-butyl-3-methylimidazolium tetrafluoroborate] have been heavily used as additives for protein crystallization,[23,24] and many commercial screening kits are already available.[25] Ionic liquids strongly affect protein surficial interactions by modifying the protein solubility, slowing the vapor transfer rate, and controlling the crystal growth kinetics.[26]

Recently, HCMs constituted of a hydrophobic membrane and ionic-liquid-based hydrogels were proposed to support protein crystallization as they preserve crystal properties. Ionic-liquid hydrogels have been developed and properly layered on hydrophobic material to form a composite material suitable for crystallization experiments at the lab scale. It was found to modify water−protein interactions, thereby altering the interaction network required for crystallization and affecting the selection mechanism of glucose isomerase polymorphs.[27]

Although DESs and ionic liquids differ substantially, they share several physicochemical properties (e.g., thermal stability, conductivity, negligible vapor pressures, and easy recycling). This prompted us to investigate the yet unexplored opportunity to use DESs to trigger protein crystallization. Spectroscopic evidence of conformational changes induced by the presence of DESs, both in their pure or hydrated forms, in bovine serum albumin and lysozyme has been already reported.[28] Results show that pure DESs reduce the protein activity by inducing a partial protein unfolding, whereas the water−DES solution preserves the protein folding, maintaining the enzymatic activity,[28] and thereby confirming the activity data recorded in the case of the photosynthetic bacterial reaction center.[14]

The presence of water plays, hence, an intriguing role. Besides influencing DES properties by modifying its supramolecular network, it has been suggested that DES components may replace water molecules involved in the protein hydration shells, thereby decreasing DES hydration.[29] Such an event, in turn, affects the protein structure, which can be significantly altered in a pure DES environment, while preserving at high hydration level of DES. Yet, in the latter case, the presence of DES molecules may alter the typical protein−water interaction network.[28]

Hydrated DESs have been investigated to collect information on the role of water molecules in the hydrogen bond network within DESs. While small quantities of water appear to strengthen the hydrogen network, higher water amounts weaken it as DES components start exhibiting a behavior closer to that of solutes in an aqueous solution.[30]

Building on this evidence, we have started an investigation pioneering protein crystallization in hydrated DESs. We attempted crystallization of three proteins in seven DESs at various hydration levels, by screening conditions previously successfully tested without DESs. We achieved crystallization of only one protein (lysozyme) in three hydrophilic DESs. Crystallographic analysis of the different crystals obtained sheds light on the intriguing interaction network between proteins and DESs.

MATERIALS AND METHODS

DES Preparation. The DESs used in this study are reported in Table 1. They were prepared by heating the corresponding individual components under stirring at 60−90 °C for 40−50 min until a clear solution was obtained.[31−34] Further details are given in the Supporting Information.

Table 1. Components and Composition of the DESs Considered in This Study

type	HBAs	HBDs	molar ratio
I	DL-menthol	L-lactic acid	1:2[a,b]
II	choline chloride	urea	1:2[c]
III	choline chloride	L-lactic acid	1:1[c]
IV	choline chloride	glycerol	1:2[c]
V	choline chloride	DL-malic acid	1:1[c]
VI	choline chloride	L-glutamic acid	1:2[c,d]
VII	choline chloride	oxalic acid	1:1[c]

[a]Hydrophobic DES. [b]L-Lactic acid: 85% (w/w) water. [c]Hydrophilic DES. [d]DES VI is a solution of the mixture at 80% (w/w) in water.

Protein Crystallization. Crystallization experiments were carried out for three test proteins: lysozyme from chicken hen egg white, dye-decolorizing peroxidases from *Rhodococcus jostii* (Dypb), and V(H) single domain of the Human Antichicken lysozyme Recombinant Antibody (HEL4). The crystallization cocktails illustrated in Table 2 were used in the absence and in the presence of the DESs shown in Table 1, at various degrees of hydration. Crystallization conditions explored solely the hydration level, while maintaining unaltered the protein and the precipitant concentration. The following conditions were used in setting the drop geometry at room temperature:

$$\begin{aligned}\text{Drop} &= (D\ \mu\text{L of protein at } P \text{ mg/mL in buffer})\\ &\quad + (D\ \mu\text{L of reservoir solution})\\ &\quad + [D\ \mu\text{L of } S\%\ \text{DES} + (100 - S)\%\ \text{water}]\\ \text{Reservoir} &= R\ \mu\text{L}\end{aligned}$$

where *D* and *R* represent the drop and the reservoir capacities, respectively, and *P* represents the protein concentration. The reservoir solution compositions were specific to each protein. The DES hydration parameter *S* was screened at the following concentrations (in %, w/w): 100, 90, 80, 60, and 0 (No-DES, control experiment). Further details can be found in the Supporting Information.

Crystal Structure Determination. Lysozyme crystals were analyzed by using the X-ray beam generated at the Diamond Light Source, beamlines I03 and I04. Data collections were carried out under cryogenic conditions (100 K) and at beam energies of 12658 eV. XDS[37] was used to perform data reduction, while POINTLESS and AIMLESS[38] were used to find the space group symmetry and to scale the diffraction data. The STARANISO server was used to merge the data in the case high data anisotropy was detected.[39] The structure was solved by molecular replacement (MR), using the REMO program[40] included in the package IL MILIONE[41] with the crystal structure 4N9R[42] as the MR model. The initial MR model was improved using the "rebuilt-in-place" function of the Phenix-Autobuild.[43,44] Structural refinement was carried out by the program phenix.refine.[45] At the end of the refinement of the protein and

https://doi.org/10.1021/acssuschemeng.1c01230
ACS Sustainable Chem. Eng. 2021, 9, 8435−8449

Table 2. Proteins Tested in This Study and Conditions Used in Crystallization Experiments

protein type	source	protein concentration P (mg/mL)	drop capacity D (μL)	reservoir capacity R (μL)	reservoir solution composition	reference
lysozyme	*Gallus gallus*	40.0	2	1000	1.2 M NaCl, 0.1 M sodium acetate, pH 4.5	21
Dypb	*Rhodococcus jostii*	10.0	1	400	2.8 M NaCl, 0.1 M sodium acetate, pH 4.5	35
HEL4	*Homo sapiens*	46.5	1	400	1.4 M $MgSO_4$, 0.1 M HEPES, pH 7.2	36

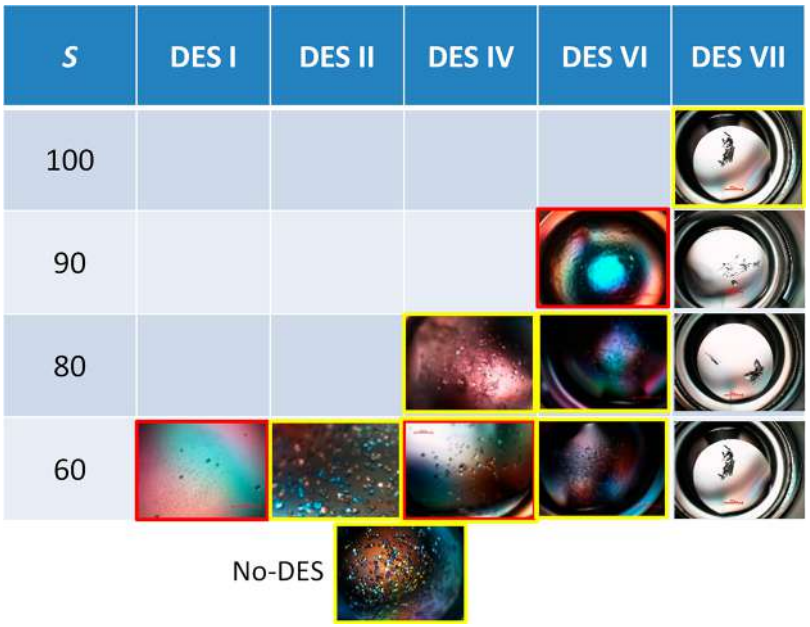

Figure 1. Crystallization experiments on hen-egg-white lysozyme. Images of the crystallization drop are reported in a table formed by DES type (rows) vs DES hydration parameter S (columns). Most of the crystals shown appeared after 1 day; images of crystals that required months to appear are contoured by a red line, and those for which X-ray structures were obtained are contoured by a yellow line.

solvent, ligands were fit in the unaccounted positive densities of the Fo-Fc map and refined with polder maps (Phenix).[46] Structural models were validated by MOLPROBITY[47] and SFCHECK.[48]

Comparative Analysis of Crystal Structures. Hen-egg white lysozyme crystal structures determined in this study were compared with 120 existing structures having $P4_32_12$ symmetry and data resolution < 1.6 Å. Water molecules, sodium and chloride ions, hydrogen atoms, and alternate configurations of residues were removed using the program Visual Molecular Dynamics (VMD).[49] VMD was also used to identify hydrogen bonds and to calculate the solvent accessibility surface area (SASA) and the protein angular value (PAV) associated to each residue. PAV values have been determined by the script TPAD,[50] according to eq 1:

$$\mathrm{PAV}_i = \frac{180}{\pi}\cos^{-1}(\cos(\psi_i + \phi_i)) \quad (1)$$

where ψ_i and ϕ_i are the backbone dihedral angles of the ith residue.[51] The PAV values lie in the range [0°, 180°] and do not suffer the typical range definition problems of angular variables.

The SASA and PAV values as a function of the residue number for each crystal structure were included in a data matrix and processed by principal component analysis (PCA) and hierarchic clustering implemented in the program RootProf.[52] Residues with missing atoms in some crystal structures (not reconstructed due to high mobility in the crystal) were excluded from the analysis. PCA results were interpreted considering score and loading plots of the first two principal components (PC1 and PC2). The score plot contains representative points of the crystal structures as described by their SASA/PAV profile. They are grouped considering their position in the plot. Key residues responsible for the separation of representative points can be identified in the loading plot, among those with the largest positive or negative values along the PC1 and/or PC2 axes.

Further comparative analyses were performed considering the root-mean-square deviation (RMSD) of C_α atoms between pairs of structures, calculated through the program SUPERPOSE,[53] and the water−protein radial distribution function, also called the surface distribution function (SDF), according to eq 2, as[54]

$$\mathrm{SDF}(r) = \frac{1}{\frac{4}{3}\pi[(R_p + r)^3 - (R_p)^3]}\frac{\mathrm{d}N(r)}{\mathrm{d}r} \quad (2)$$

where r is the water−protein distance, $N(r)$ is the number of water molecules at distance r, and R_p is the radius of gyration of the protein, calculated from the lysozyme structural model. Distances between 0 and 7 Å, with a step of 0.05 Å, were considered. Hydrogen atoms, ligands, and ions present in the PDB file were excluded from the analysis. SDFs were normalized to the area under the curve, to account for the dependence of the number of water molecules in crystal structures on data resolution. The programs PyMOL[55] and RootProf[52] were used for these calculations. The first one has been used in script mode to calculate the number of water molecules found within each distance r from the protein.

RESULTS AND DISCUSSION

Crystallization Experiments. Figure 1 shows images of the crystallization plates in which crystals were grown during a six-month period ordered by the DES type and the hydration level. Most of the crystals shown appeared after 1 day; those contoured by a red line required months to appear.

https://doi.org/10.1021/acssuschemeng.1c01230
ACS Sustainable Chem. Eng. 2021, 9, 8435−8449

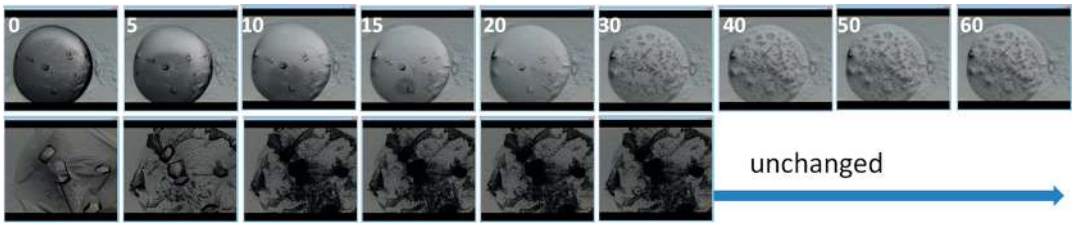

Figure 2. Time course of the crystal dissolution tests performed on two crystallization drops exposed to the air containing lysozyme crystals grown in the presence of DES VI (upper row) and under No-DES conditions (lower row). Experiments were performed at room temperature. The time (in min) from the start of the exposure is shown.

Table 3. Data Collection and Refinement Statistics of the Crystal Structures of Hen-Egg White Lysozyme Determined in This Study[a]

	No-DES	DESII_60	DESIV_60	DESIV_80	DESVI_60	DESVI_80
			Data Collection			
cell constants *a*, *c* (Å)	78.953, 37.304	80.050, 36.769	78.230, 37.209	78.901, 37.124	78.789, 36.959	78.964, 37.093
cell volume (Å^3)	232537	235616	227717	231111	229430	231286
resolution range (Å)	39.48−1.20 (1.22−1.20)	56.59−2.20 (2.26−2.20)	30.87−2.50 (2.59−2.50)	55.79−1.30 (1.32−1.30)	55.71−1.30 (1.32−1.30)	27.92−1.30 (1.32−1.30)
completeness (%)	99.3 (99.9)	99.9 (99.4)	80.9 (83.5)	99.9 (100.0)	94.0 (100.0)	99.6 (94.8)
multiplicity	6.8 (6.7)	24.9 (26.2)	2.6 (2.6)	6.8 (6.4)	7.0 (6.8)	21.5 (6.8)
number of unique reflections	37171 (1805)	6448 (496)	3487 (350)	29376 (1470)	27466 (1376)	29313 (1464)
R merge (%)	6.3 (58.3)	14.2 (57.8)	11.5 (26.3)	6.3 (54.9)	8.5 (58.8)	9.0 (33.0)
R meas (%)	6.8 (63.0)	14.5 (59.0)	13.9 (32.2)	6.9 (59.8)	9.1 (63.6)	9.2 (35.7)
$\langle I/\sigma(I)\rangle$	10.8 (2.1)	14.2 (5.8)	5.1 (2.7)	13.5 (2.6)	10.7 (2.5)	25.9 (4.9)
$CC_{1/2}$	0.998 (0.873)	0.999 (0.983)	0.976 (0.891)	0.998 (0.909)	0.998 (0.897)	0.999 (0.934)
Wilson B-factor (Å^2)	17.3	32.0	42.2	16.1	16.1	15.8
			Refinement			
Rwork/Rfree (%)	13.2/15.7 (20.9/22.9)	17.9/22.6 (20.7/26.1)	20.1/26.0 (27.0/32.1)	12.7/16.4 (17.8/22.8)	12.6/15.4 (16.1/21.1)	11.0/14.3 (14.0/19.3)
MolProbity score	1.6	1.0	1.3	1.8	1.7	1.4
Clashscore	5.7	2.3	5.9	10.1	9.8	6.8
average B-factor (Å^2) (protein atoms)	15.9	21.4	34.6	11.6	11.6	11.0
average B-factor (Å^2)/occupancy (water atoms)	30.1/0.91	27.1/0.96	37.4/0.98	26.4/0.85	25.0/0.85	26.8/0.88
protein atoms	1320	1056	1003	1142	1133	1324
water molecules	194	100	53	227	201	217
RMSD bonds length (Å)	0.009	0.006	0.007	0.007	0.008	0.007
RMSD bond angles (deg)	1.0	1.1	1.0	1.0	1.1	0.9
Ramachandran favored (%)	99.2	99.2	99.2	99.2	99.2	98.4
Ramachandran outlier (%)	0.0	0.0	0.0	0.0	1.6	0.8
DPI (coordinate error) (Å)[56]	0.05	0.21	0.38	0.06	0.06	0.05

[a]Outer shell statistics are in round brackets. No X-ray data were collected for DES I (S = 60) and for DES VI (S = 90) since crystals were too small and the mother liquor too viscous, respectively.

Lysozyme crystallizes in five out of seven of the explored DESs, the most suitable one being DES VI (2:1 choline chloride/glutamic acid) where crystals were grown at very high DES contents (S = 60, 80, 90). Crystals obtained by using DES VII had different shapes and sizes, and their nucleation was independent of the hydration level. In all cases, crystallization appeared significantly hampered in the presence of DES. As expected, the viscosity of the mother liquor (and consequently the mobility of the crystals) increased by increasing the DES concentration. No crystals were obtained by using DES III and DES V. It is worth noting that DES I, II, IV, and VI, each one containing one of the components composing DES III, were allowed to get crystals.

The other two proteins tested (Dypb and HEL4) produced crystals only under No-DES conditions and when using DES VII only (Figure S1). Similarly to the case of lysozyme, crystals obtained by using DES VII have very different shapes and sizes with respect to those grown under No-DES conditions (more details in the Supporting Information), and their nucleation was independent of the hydration level.

Crystal Dissolution Experiments. Some crystallization conditions were used to perform the protein crystal dissolution tests. It has been verified that individual lysozyme crystals were fished from the crystallization drop and, once immersed in 10 μL of ultrapure water (Milli-Q), dissolved in about 10 min, regardless of the growth conditions.

When the entire crystallization drop was exposed to air, the presence of DES slowed down drop evaporation compared to No-DES conditions, and preserved the lysozyme crystals for at least 1 h. The different behavior is illustrated in Figure 2. Without DES, crystals darkened within 10 min from the beginning of the experiment, a condition that could lead to a

https://doi.org/10.1021/acssuschemeng.1c01230
ACS Sustainable Chem. Eng. 2021, 9, 8435−8449

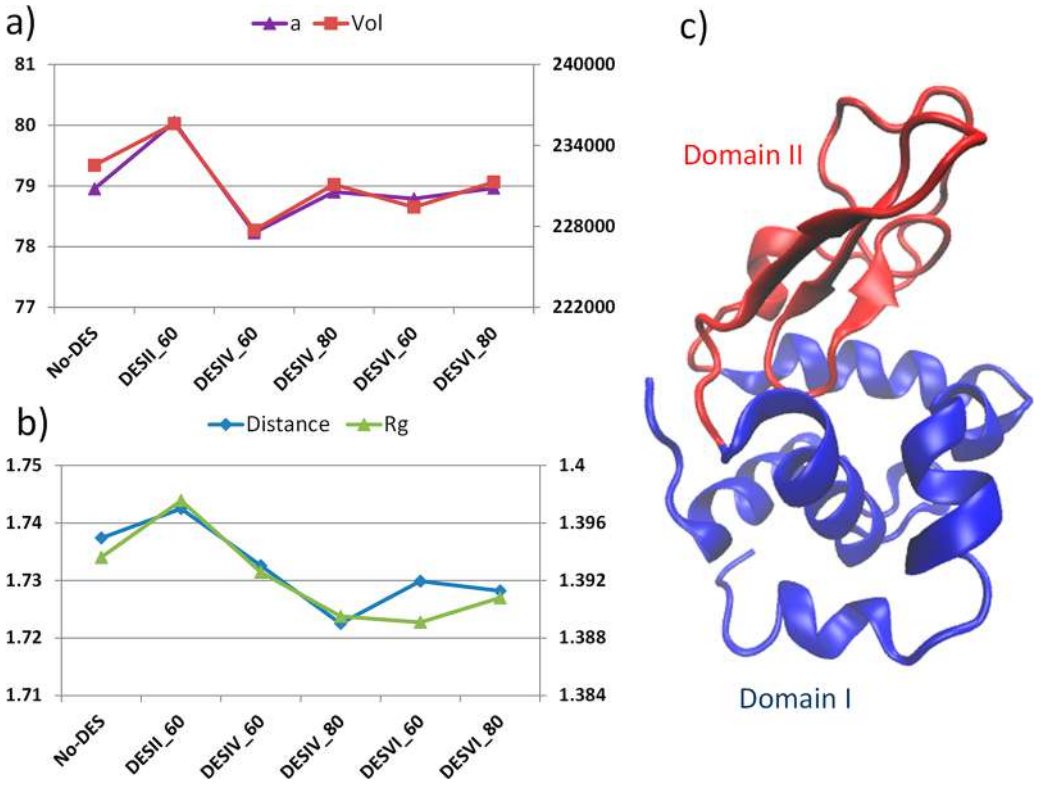

Figure 3. Cell parameter *a* (left axis) and cell volume (right axis) (a), distance between Domain I and Domain II (left axis) and gyration radius (right axis) (b) of the crystal structures determined in this study. Domain I and domain II of lysozyme, consisting, respectively, of residues 1−38 and 88−129 and of residues 39−87 are shown (c).

Table 4. B Factor Averaged on Non-hydrogen Atoms (Å^2) and Crystallographic Occupancy of Ligands Reconstructed in the Crystal Structures of Hen-Egg White Lysozyme Determined in This Study[a]

name	No-DES	DESII_60	DESIV_60	DESIV_80	DESVI_60	DESVI_80
ACT	20, 0.77	21, 0.84	25, 0.70	20, 0.87	14, 0.75	16, 0.90
CHT1		46, 0.84	65, 0.91	46, 0.95	39, 0.89	23, 0.44
CHT2		34, 0.73	52, 0.80	43, 0.65	38, 0.92	36, 1.00
URE1		19, 0.97				
URE2		19, 0.50				
URE3		30, 0.91				
URE4		24, 0.50				

[a]Ligand names: choline (CHT), urea (URE), and acetate ion (ACT).

loss of protein functionality. The ability of DES to protect protein crystals from rapid dissolution can be exploited in biotechnological applications involving enzymes in crystalline form.

Crystal Structure Analysis. The crystal structures of hen-egg-white lysozyme crystallized in the following conditions: *S* = 60 for DES II (DESII_60), *S* = 60 and 80 for DES IV (DESIV_60 and DESIV_80), and DES VI (DESVI_60 and DESVI_80). A further crystal structure crystallized under No-DES conditions has also been determined for comparison studies. All crystal structures have $P4_32_12$ symmetry. Data collection and refinement statistics have been included in Table 3.

By analyzing the data in Table 3, it can be noted that, compared with No-DES, two data sets (DESII_60 and DESIV_60) have lower resolution, then higher positional errors (>0.20 Å), higher thermal fluctuations (average B factor for protein atoms > 20 Å^2), and a lower number of water molecules. The data set DESVI_80 has the highest multiplicity and, thus, the best crystallographic and refinement statistics. Among the data sets with comparable resolutions and multiplicity, DES VI_60 and DESIV_80 have systematically better refinement statistics than No-DES (lower Rwork/Rfree, B factors, and RMSDs and higher validation scores). Interestingly, these data sets have also a higher number of water molecules with respect to the crystal grown without DES, suggesting a positive effect of DESs in the hydration of the protein in the crystal form.

Contrary to data resolution, which is not affected by DES composition and hydration, the unit cell size shows a dependence on DES. Particularly, DES II induces the largest deviations of crystal cell parameters, with the cell volume increasing by 3078 Å^3 compared to No-DES, and systematically decreases in the presence of DES IV and DES VI.

The variations of the cell volume induced by the presence of DESs are strictly related to those of the largest cell parameter *a* (Figure 3a). At the molecular level, the characteristic size of the lysozyme undergoes similar variations depending on the

https://doi.org/10.1021/acssuschemeng.1c01230
ACS Sustainable Chem. Eng. 2021, 9, 8435−8449

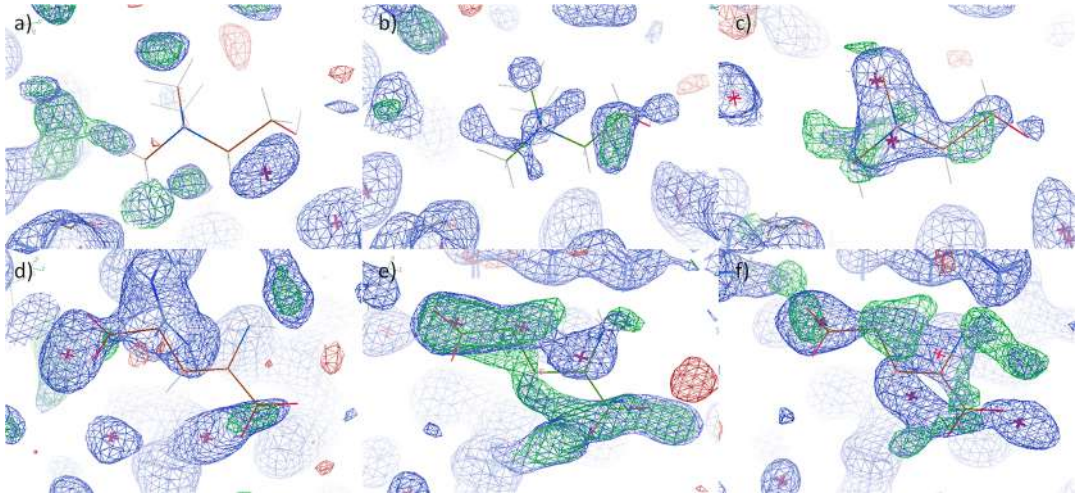

Figure 4. Electron density 2Fo-Fc (blue, contoured at 0.5σ) and Fo-Fc (green-red, contoured at 3.0σ) of the CHT3 (a, b, c) and GLU (d, e, f) sites of No-DES (a, d), DESVI_60 (b, e), and DESVI_80 (c, f). The choline and glutamic acid atomic models are superposed on the figures to guide the eye, and Fc values are calculated without considering these molecules.

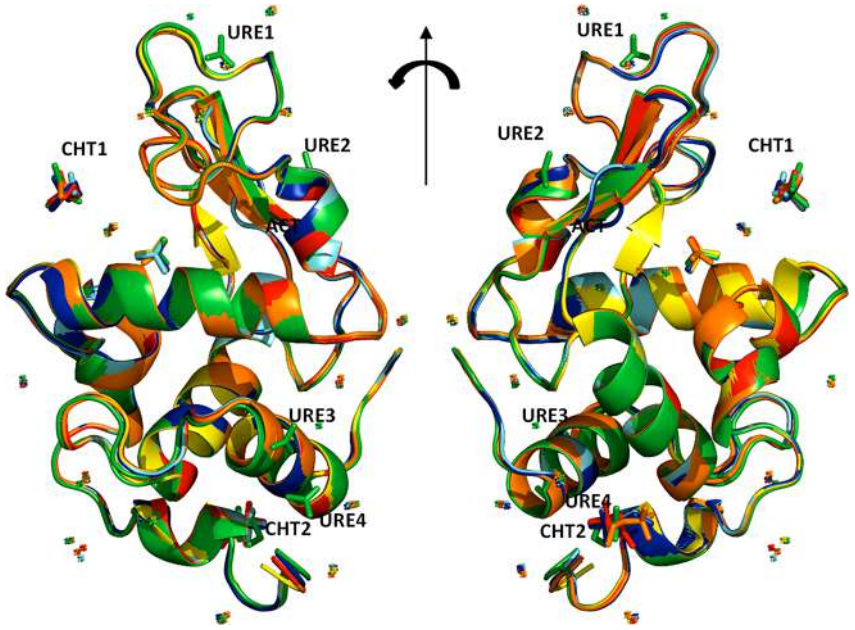

Figure 5. Superposed crystal structures of hen-egg white lysozyme determined: No-DES (yellow), DESII_60 (green), DESIV_60 (orange), DESIV_80 (red), DESVI_60 (cyan), and DESVI_80 (blue) according to the nomenclature of Table 1. Reconstructed ligands are acetate ion (ACT), choline (CHT), and urea (URE). Chloride and sodium ions are shown as stars.

solvent type. In fact, the distance between the centers of the two domains describing the lysozyme tertiary structure (Figure 3b) and the radius of gyration of the whole protein, as calculated for the crystal structures determined in this study, are larger in DES II and smaller in DES IV and DES VI with respect to No-DES (Figure 3c). An increase in the size on going from No-DES to DES II has also been observed for the lysozyme simulated in a solvation box constituted by a mixture of reline and water,[57] and the experimental values of the domain I−II distance and the gyration radius determined in this study are consistent with those predicted by Kumari et al. for highly diluted systems.[57] Therefore, X-ray diffraction data show that lysozyme does not denature in the eutectic mixture of urea as it would have happened in the presence of urea as it is. Most probably, urea/ChCl interactions prevent destabilization of the protein. On the other hand, we found that shape variations induced by this DES on the protein in solution also occur in the solid state, as a result of a rearrangement of crystal packing.

A number of ligands were reconstructed in the crystal structures, and their main features are given in Table 4. All the atoms of each ligand have been constrained to the same occupancy value.

In addition, two putative ligand sites have been identified in crystals containing DES VI, as shown in Figure 4: a third choline (CHT3) site and a glutamic acid (GLU) site. Electron density maps in these sites are absent in No-DES, barely hinted at in DESVI_60, and well-defined in DESVI_80. In addition, Arg128 changes its side-chain conformation, occupying the GLU site in No-DES, and leaving it free in crystal structures containing DES VI. Despite this evidence, fitting choline and glutamic acid molecules in the electron density of these

https://doi.org/10.1021/acssuschemeng.1c01230
ACS Sustainable Chem. Eng. 2021, 9, 8435−8449

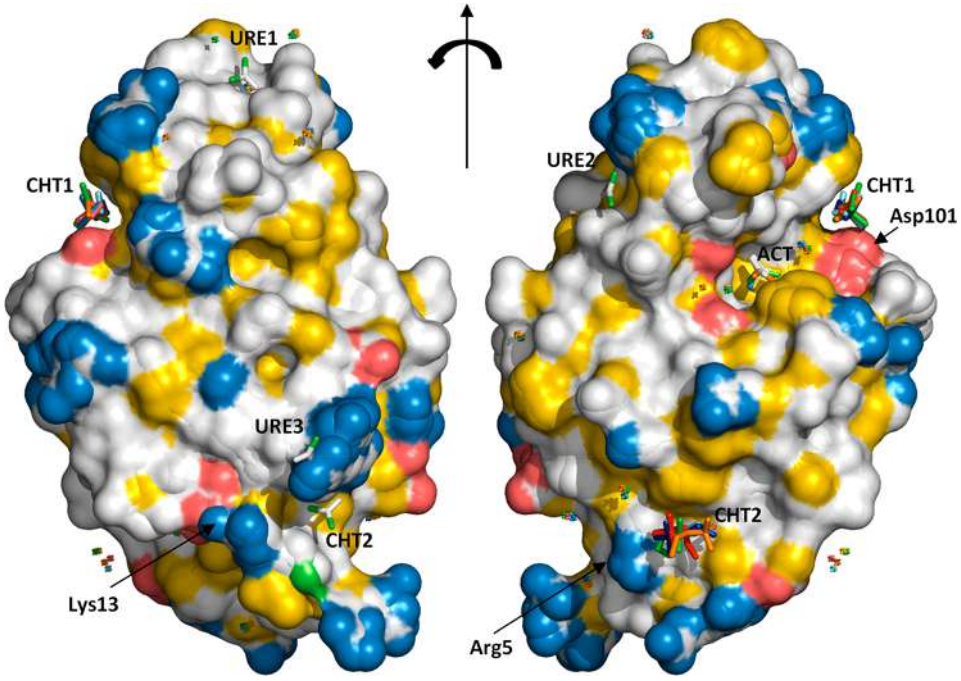

Figure 6. Surface representation of crystal structures of hen-egg white lysozyme, colored according to the YRB scheme: hydrocarbon groups without polar substitutions are yellow; negatively charged oxygens of glutamate and aspartate are red; nitrogens of positively charged functional groups of lysine and arginine are blue; and all remaining atoms including the polar backbone are white. The coloring reflects the typical charges at physiological pH and has been obtained by using a PyMOL script.[59] Ligand nomenclature as in Table 4. Charged residues interacting with ligands are highlighted by arrows (distance < 5 Å).

structures is not robust, i.e., electron densities are too weak to justify ligand positioning (Figure S2), so that corresponding ligands could not be validated. The electron density maps in these two sites have been accounted for by means of closely spaced water molecules (Figure 4).

Crystals in DES VII produced a diffraction pattern typical of salts. Diffraction experiments on several crystals obtained from DES VII at different hydration levels show the structure of sodium hydrogen oxalate (see details in the Supporting Information).

X-ray diffraction has shown that crystals obtained from crystallization experiments performed by using Dypb and HEL4 are made of protein only in the case of No-DES conditions, whereas the remaining ones (crystals grown in DES VII) are made of salt. We can envisage the same effect as seen in the case of lysozyme; i.e., the high concentration of sodium and magnesium ions has led to the formation of salt crystals in DES VII for Dypb and HEL4 proteins, respectively.

Crystal structures DESII_60, DESIV_80, and DESVI_80 were deposited to the Protein Data Bank, with accession codes 7b9j, 7baz, and 7bb1 respectively, as representative structures of hen-egg white lysozyme crystallized in DES.

Comparative Analysis of Crystal Structures Obtained in DESs. *Analysis of the Ligands.* The structural models of lysozyme determined in this study are shown superposed in Figure 5 and separately in Figure S3. All structures, including No-DES, show an acetate ion ACT sitting in the same site in agreement with most of the lysozyme crystal structures obtained in the presence of sodium acetate and deposited in the PDB. The X-ray structures of crystals obtained from the binary DESs (1:2 mol mol^{-1}) choline chloride:urea, choline chloride:glycerol, and choline chloride:glutamic acid show the presence of two choline (CHT) binding sites (Figure 7), with choline always showing a similar conformation. The second component of the DES, the H-bond acceptor, is only present in the structures with DES II, where four urea molecules interact with the protein and its solvation shell (Figure 8). A putative glutamic acid site can be glimpsed in DESVI_60 and DESVI_80 crystal structures (Figure 4).

The presence of both DES components in the crystal structure of DES II could be related to a weaker interaction among its components, when compared to the cases of DESs IV and VI. Indeed, by considering the DES components interacting in their molar ratio, we observed that up to 10 different H-bonds can be formed in the case of DES II, up to 12 in the case of DES IV, and up to 14 in the case of DES VI. Moreover, Coulomb interactions occur in this latter DES, due to the presence of opposite charges on glutamic acid and the choline ion. Therefore, components of DES IV and DES VI have a larger number of mutual interactions than in the case of DES II, and thus they are less prone to interact with the protein.

While giving a rationale about the presence of the second DES component in the crystal structure, the above argument could also explain the DES efficiency (DES II < DES IV < DES VI) in triggering lysozyme crystallization (Figure 2). Based on noncovalent, mutual interaction (H-bonds and ion−ion interactions) among DES components (Figure S5), the employed DESs can be grouped as follow: (a) DESs whose components show the highest number of mutual interactions (DES IV and DES VI), (b) DESs whose components show the lowest number of interactions (DES I, DES III, and DES VII), and (c) DESs for which the number of interactions is in between the above groups (DES II). As a consequence, components of DES IV and DES VI and, to a lesser extent, of DES II will interact much more with each other rather than

https://doi.org/10.1021/acssuschemeng.1c01230
ACS Sustainable Chem. Eng. 2021, 9, 8435−8449

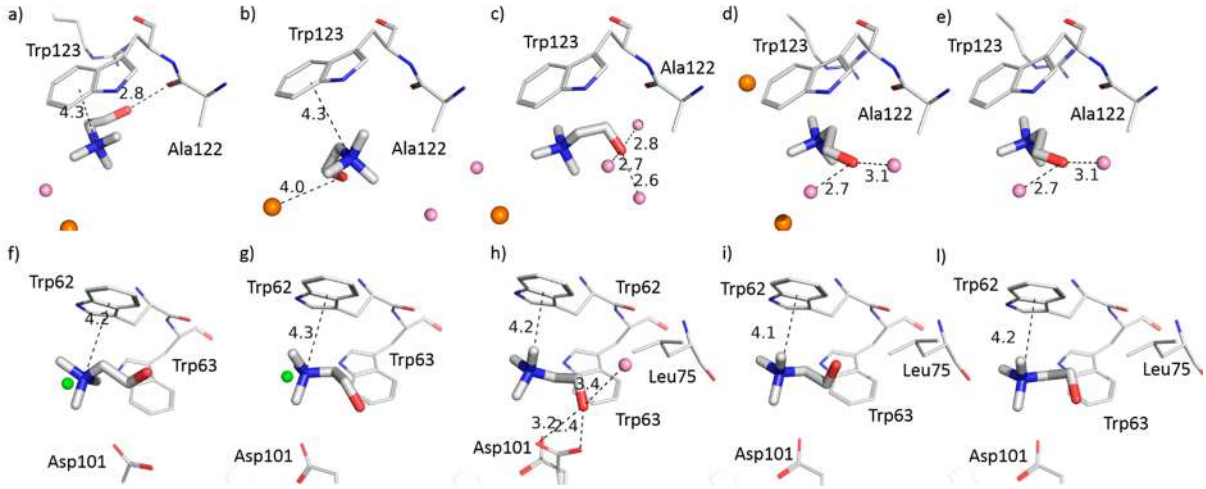

Figure 7. Choline sites CHT1 (a–e) and CHT2 (f–l) of all crystal structures containing DES (left to right: DESII_60, DESIV_60, DESIV_80, DESVI_60, DESVI_80). Residues, chloride ions (green spheres), sodium ions (orange spheres), and water molecules (pink spheres) having distances less than 4 Å from non-hydrogen atoms of the choline ion are shown. Hydrogen bonds (<3.5 Å), ion-dipole interactions (<4.0 Å), and the cation–π interaction (<4.5 Å) are highlighted with dashed lines. Distance values are reported in angstroms.

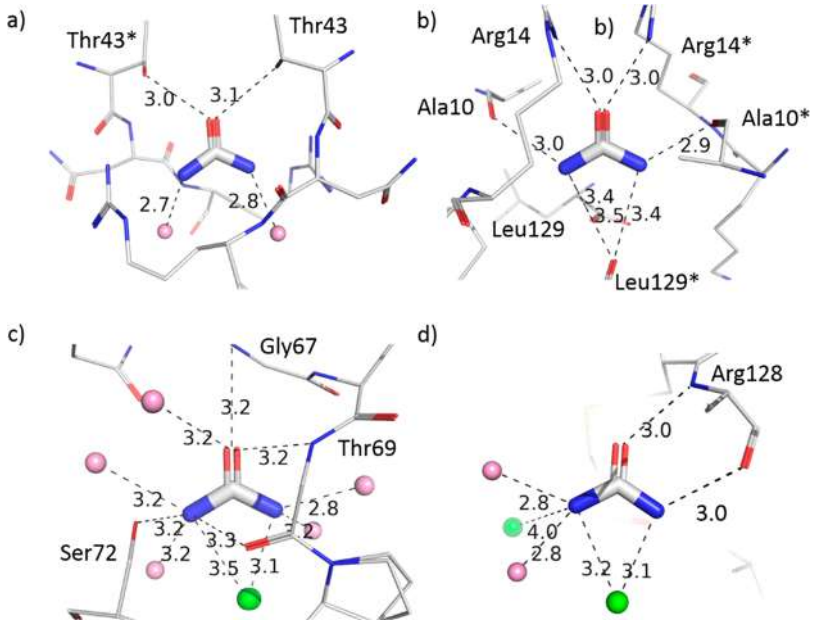

Figure 8. URE sites in the DESII_60 crystal structure: URE1 (a), URE2 (b), URE3 (c), URE4 (d). Residues, chloride ions (green spheres), and water molecules (pink spheres) having distances less than 4 Å from non-hydrogen atoms of the urea molecule are shown. Asterisks denote residues belonging to symmetry-equivalent units. Hydrogen bonds (<3.5 Å), ion-dipole interactions (<4.0 Å), and the cation–π interaction (<4.5 Å) are highlighted with dashed lines. Distance values are reported in angstroms.

with the protein, while those belonging to DES I, DES III, DES V, and DES VII will be much more prone to interact with the protein. In the latter case, this would decrease the electrostatic free energy of the protein, while increasing the activity of the solvent and, thus, the protein solubility (salting-in effect). In such conditions, the solution is undersaturated, and the crystallization process will be hindered as the formation of a proper network of protein–protein contacts will be prevented. Conversely, DESs characterized by strong interactions among their components will allow protein crystallization because protein solubility will not be affected. Thus, a subtle interplay between two opposite phenomena could explain why lysozyme crystals are formed in DES II only at higher hydration levels (S = 60) (strong protein–DES interactions need to be attenuated), while they occur at lower hydration levels in DES IV (S = 60 and 80) and even more in DES VI (S = 60, 80, 90), most probably as they both favor the right balance of interactions between DES–protein and protein–protein.

DES components found in the crystal structure interact with protein residues, while there is no evidence of their mutual interactions. This confirms the weakening of the strong inter- and intramolecular interactions between DES components by water addiction[58] and the fundamental role of the protein–DES interactions in the crystallization process.

Analysis of the Surface Charge. Surface charge analysis, shown in Figure 6, unveils the relevance of the hydrophobicity and charge in the interactions with DES components. The CHT1 and CHT2 sites are located in hydrophobic pockets,

https://doi.org/10.1021/acssuschemeng.1c01230
ACS Sustainable Chem. Eng. 2021, 9, 8435–8449

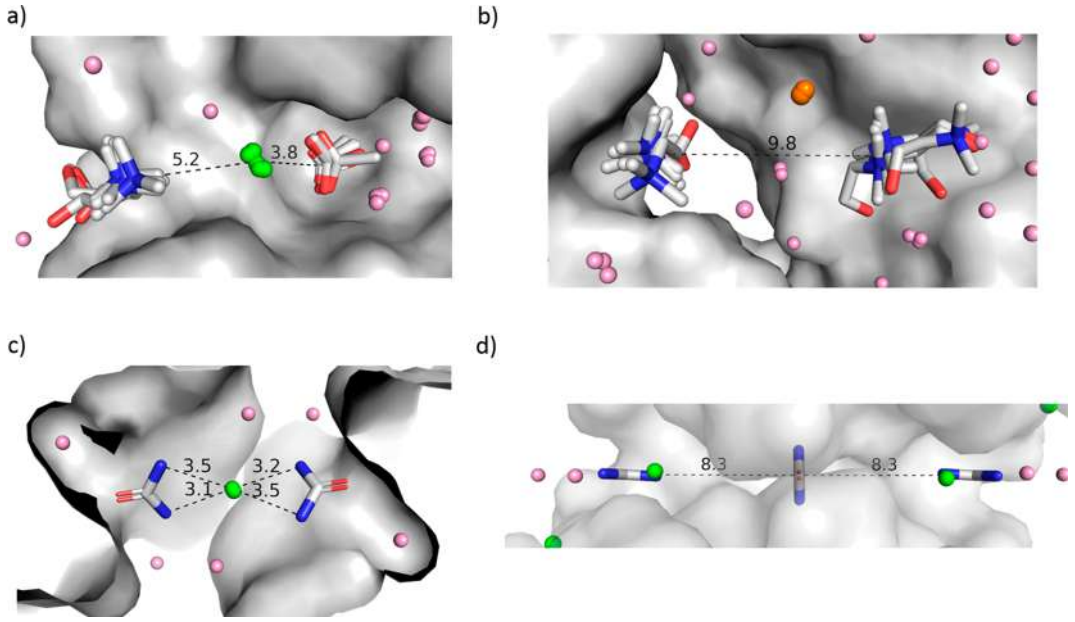

Figure 9. Neighboring ligands. (a) CHT1 and ACT. The distance between the centroid calculated among the nitrogen atoms of each CHT1 molecule and that calculated among the chlorine atoms in the middle of the figure is shown along with the distance between this last centroid and that calculated among the oxygen atoms of the ACT molecules. (b) CHT1 and CHT2 (the distance between the centroid of the CHT1 molecules and the centroid of the CHT2 molecules is shown). (c) Interactions between two symmetrically equivalent URE1 of the DESII_60 crystal structures (the distance related to the ion−ion interaction between the chloride atom and the nitrogen atoms of the URE1 molecules are shown). (d) URE4 and two symmetrically equivalent URE3 of the DESII_60 crystal structure (the distance between the centroid of the URE4 molecules and the centroids related to URE3 molecules are shown). URE and CHT molecules are shown in stick representation. Chloride ions, sodium ions, and water molecules are shown as green, orange, and pink spheres, respectively. Distance values are reported in angstroms. The solvent accessible surface of the lysozyme protein related to the DESII_60 crystal structure is also shown in each figure.

delimited by the negatively charged residue Asp101 and the positively charged residue Arg5. Urea and acetate ion molecules are located in hydrophobic pockets; urea is exposed to the solvent, while the acetate binding site is buried. Further details relative to the ligands are discussed below.

Choline Sites. The two choline sites CHT1 and CHT2 are shown in higher detail in Figure 7. Choline ions in CHT1 (Figure 7a) interact with Trp62, through a cation−π interaction, with Asp101, through a hydrogen bond, and with Asp119, through a water-mediated hydrogen bond. Other close (<4 Å) residues are Trp63 and Leu75. Residues Gln121 and Leu75 from a symmetry-equivalent protein unit are close to the choline ion of DESII_60, which is slightly shifted with respect to those of other DES structures. A chloride atom completes the site, located at a distance of 3.7 Å from the choline ion. The CHT2 site (Figure 7b) is also dominated by a cation−π interaction between choline and Trp123. Other interactions are a hydrogen bond with the main chain of Ala122 and a water-mediated hydrogen bond with Gly117, this latter present only in crystal structures with DES VI. Two sodium ions are close to the choline ion, at a distance of about 3.8 Å. It is worth noting that both chloride and sodium ions in the choline sites are also present in the No-DES crystal structure and in many known lysozyme structures. Thus, their presence is not related to DES. Many water molecules surround the choline ions in both sites.

Urea Sites. Four urea binding sites have been found in the DESII_60 crystal structure (Figure 8). URE1 interacts with residues Asn65, Gly67, Arg68, and Thr69 and a chloride atom, whereas URE3 has a poorer coordination sphere that includes the residue Arg128 and one chloride atoms (which is only present in the DESII_60 crystal structure). URE2 and URE4 are on special positions; namely, they are crossed by a binary axis, so that they interact with pairs of symmetry-equivalent residues. The involved residues are Thr43 and Arg45 for URE2 and Ala10, Arg14, and Leu129 for URE4.

Interaction Network. An extended interaction network appears to connect the DES components positioned at the border of the asymmetric unit. In all DES-containing crystal structures the choline ions in the CHT1 and CHT2 sites are about 7 Å apart (Figure 9a), and the choline ion in the CHT1 site interacts with the acetate ion (ACT), through a chloride ion placed halfway between the two (Figure 9b). Figure 9c shows the interaction between the urea molecule in the URE1 site of DESII_60 and its symmetrical equivalent, placed 7.6 Å apart and having the plane rotated by ∼30°. Although our experiment does not provide information on hydrogen atoms, we expect that, similarly to what happens in the case of the water solution of urea, URE1 and URE2 are protonated. This is suggested by the presence of a chloride ion located halfway between the two urea molecules, which very unlikely interacts with such molecules in their deprotonated states. It is interesting to note that, in No-DES and the other DES-containing crystal structures, such a chloride ion is shifted and occupies the position of two symmetrically equivalent urea molecules. The urea molecule in the URE4 site is connected with two symmetrically equivalent urea molecules in the URE3 site, placed orthogonally and 6.9 Å apart from it (Figure 9d).

Analysis of the Backbone Atoms. A comparative analysis on lysozyme C_α atoms, carried out by using Cartesian (RMSD) and dihedral angle (PAV) descriptors, shows that structures formed in DES have substantial deviations from the No-DES structure only in the last two C-term residues (Figures S6 and S7). The average RMSDs are 0.33 Å for

https://doi.org/10.1021/acssuschemeng.1c01230
ACS Sustainable Chem. Eng. 2021, 9, 8435−8449

DESII_60 and below 0.23 Å for crystal structures containing DES IV and DES VI (Figure S6). Even the analysis of the backbone dihedral angles highlights the high similarity of the crystal structures containing DES IV and DES VI (Figure S7). *Crystallized proteins, hence, do not show significant conformational changes in any secondary structural element induced by DES.*

Analysis of the Solvent Accessibility. Differences that are more significant are evidenced by considering the solvent accessibility of the residues, calculated in the presence of ligands. PCA separates the No-DES and DESII_60 crystal structures from those containing DESIV and DESVI along the first principal component (PC1) (Figure S8). Differences are due to the presence of DES components, which reduce the solvent accessibility of the interacting residues. In order of relevance, they are Trp62, Leu75, and Asp101 in the CHT1 site, Arg14 in the URE4 site, Trp123 in the CHT2 site, Arg45 in the URE2 site, and Ser72 in the URE1 site. They are highlighted in Figure 10, colored according to the PC1 loading

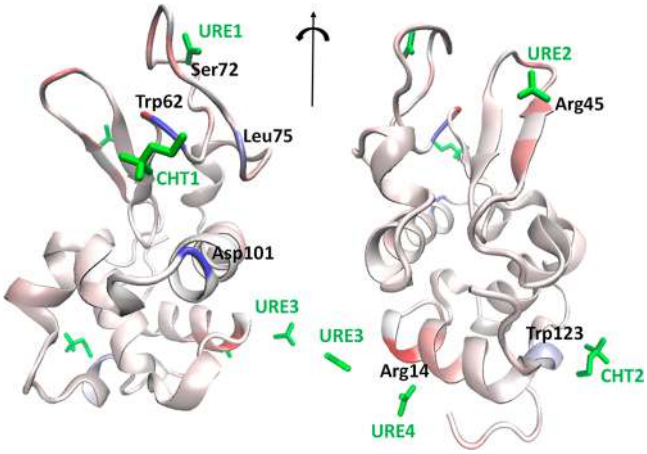

Figure 10. Crystal structure of DESII_60 colored according to the loading values of the first principal component determined by PCA applied to SASA values of the crystal structures determined in this study. Residues having the largest positive (red) and negative (blue) loadings and DES components found in the crystal structures (green) are indicated.

values. It is worth noting that a similar PCA separation is obtained if the ligands are not considered in the SASA calculation (Figure S9). *Thus, the presence of DES influences the solvent accessibility and the side-chain conformation of residues interacting with DES components.*

Analysis of the Hydration Shell. Hydration waters in crystal structures play a critical role by contributing to the protein folding, stability, and dynamics. The experimental properties of hydration waters have been studied using the surface distribution function (SDF), which describes the density of the water molecules as a function of the distance (r) from the closest non-hydrogen atom of the protein.[54] SDF calculated from the DES crystal structure does not show significant differences from the No-DES structure (Figure S10): all show the characteristic SDF peak located at r = 2.75 Å, representing the first hydration shells around the protein.[54] The shape of the SDF peak is broader for DESII_60 and DESIV_60, as an effect of the lower data resolution of these two crystal structures. *DESs, therefore, do not cause remarkable global changes in the distribution of hydration waters.*

Comparison with Other Crystal Structures. There is a single crystal structure of lysozyme containing choline chloride in the PDB (code 4aga).[60] It was crystallized by using the ionic liquid 1-butyl-3-methylimidazolium trifluoromethanesulfonate-choline as the additive, the latter being shown superposed to those determined in this study in Figure 11. 4aga has the

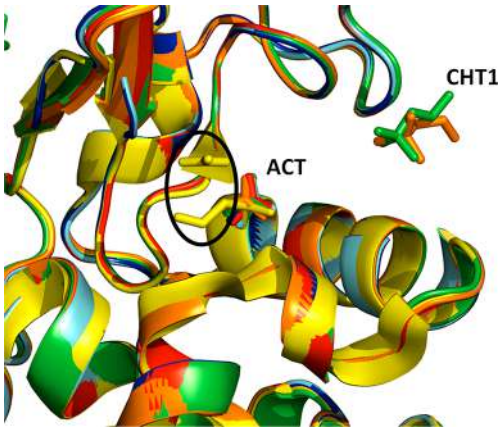

Figure 11. Superposed crystal structures of hen-egg white lysozyme determined in the present study: DESII_60 (green), DESIV_60 (orange), DESIV_80 (red), DESVI_60 (cyan), and DESVI_80 (blue) with the crystal structure with PDB code 4aga (yellow). Reconstructed ligands are CHT and ACT. The positioning of the acetate ion and choline molecule in the crystal structure 4aga is highlighted by a black ellipse.

choline ion placed in the site systematically occupied by an acetate ion in all the crystal structures considered in this study, including that crystallized without DES. In addition, it has an acetate ion shifted by 4 Å from the ACT site and no choline molecule in the CHT1 or CHT2 sites, although a careful analysis of the electron density map would suggest their presence (Figure S11). Moreover, the presence of DES did not result in a significant contraction of the unit cell upon binding to choline and acetate, as instead observed for 4aga (6470 Å^3). This can be attributed to a possible desiccation/dehydration effect of the ionic liquid additive.[60]

The interaction of urea with lysozyme has been investigated in the framework of denaturation studies, where lysozyme crystals were soaked in >4.5 M urea solutions. Crystal structures obtained at different soaking times are available for lysozyme crystallized in $P4_32_12$ (PDB codes 5i4x, 5i4y, 5i53, 5i54)[61] and in $P1$ (PDB code 2f30).[62] All the four URE sites found in DESII_60 are occupied in the $P4_32_12$ crystal structures already at the first stages of soaking (2 h), while the urea molecules in the $P1$ crystal structure do not overlap with those found in DESII_60. This confirms that crystal packing plays a key role in determining the binding of solvent molecules. It should be noted that all these structures have a urea molecule replacing the acetate ion in our ACT site. It is also interesting to note that the structural alterations reported as the onset of denaturation[61] are not present in DESII_60, because our URE site does not coincide with any of the urea binding sites involved in the proposed mechanism of denaturation.

A comprehensive comparison has been carried out by considering a representative set of 120 lysozyme crystal structures. In this context, the comparative analysis based on PAV profiles is not able to separate DES-containing structures

https://doi.org/10.1021/acssuschemeng.1c01230
ACS Sustainable Chem. Eng. 2021, 9, 8435−8449

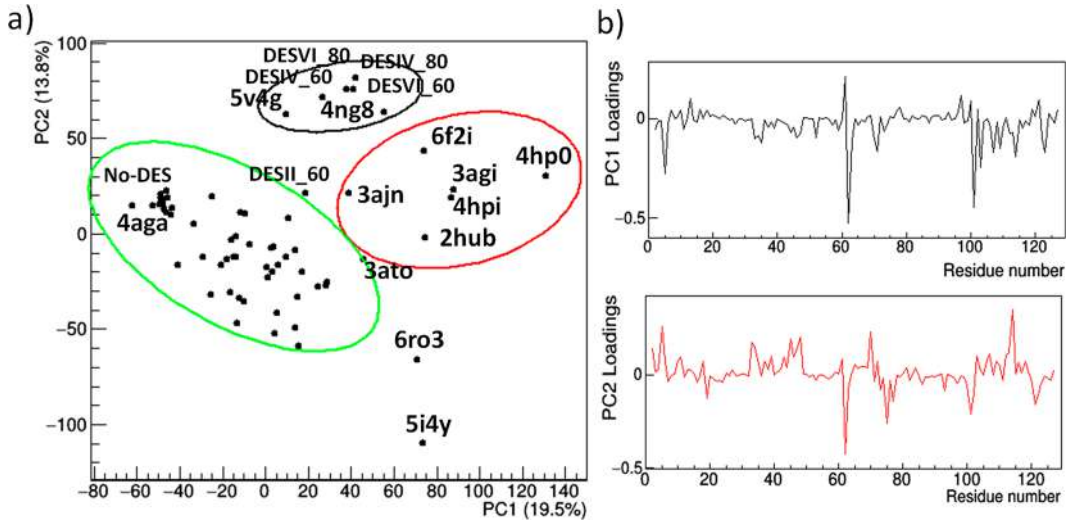

Figure 12. Results of the comparative analysis of the SASA profiles of a set of 120 lysozyme crystal structures. (a) Score plot of the first two principal components, where representative points are grouped according to a hierarchic clustering algorithm. The percentage of the total data variance explained by each principal component is reported on the axes, with ellipses representing the 85% confidence level. PDB codes associated with representative points are also reported. (b) Loading plot of the same principal components, where the residues relevant for discrimination have the largest positive or negative values.

from the No-DES structure (Figure S12), confirming that perturbations in backbone conformation induced by DES are not significant. On the contrary, crystal structures involved in unfolding by urea fall into another cluster, confirming that the presence of DES containing urea in the crystallization cocktail does not alter the backbone conformation. Residues responsible for the separation of lysozyme crystal structures according to backbone deviations are highlighted in Figure S13, as determined by the PCA loadings.

The PCA-based comparative analysis applied to SASA determinations (Figure 12) shows a separation of crystal structures in three clusters. This is due to the presence of ligands in specific sites. Residues having the larger loading values are those located in the CHT1 site (Trp62, Trp63, Asp101) and in the CHT2 site (Arg5, Trp123). These two sites are hence important to characterize the solvent exposure and are mainly responsible for the cluster separation. The cluster containing the No-DES and 4aga includes crystal structures that have no ligands or ligands not located in the CHT1 or CHT2 sites. Crystal structures populating the remaining clusters have, instead, at least one of the two sites occupied by a ligand. DES-containing structures show, among others, specific solvent accessibility properties because of the presence of choline ions. Thus, they can all be grouped in the same cluster, together with the crystal structures 4ng8 and 5v4g. The third cluster comprises crystal structures having ligands determining a different solvent accessibility of the CHT1 and CHT2 sites with respect to that of DES-containing structures. Similar PCA results are obtained when SASAs are calculated without considering ligands (Figure S14), thereby confirming the footprint left from ligands on the side-chain conformation of neighboring residues.

Ligands determining the SASA separation in the above-mentioned structures are summarized in Table 5. It is interesting to note that 5i4y is the only structure among those reported[61] having a urea molecule in the CHT2 site. As for 3ajn, 3agi, and 3ato, it was found that ligand binding has the effect of decreasing the SASA of aromatic residues while increasing that of charged residues. By preventing intermolecular hydrophobic interactions through hydrophobic regions of the lysozyme surface, these changes were found to increase the protein solubility.[63,64] In our study, we have found a similar effect, involving aromatic (Trp62, Trp63, Trp123) and charged (Arg61, Arg5) residues lying in the CHT1 and CHT2 sites. Thus, choline ions determine unique changes in solvent accessibility of aromatic residues at specific sites (CHT1 and CHT2), which might increase the protein solubility,[63] thereby hindering the protein aggregation.[64] This fact strongly suggests that *DES can locally modulate the structure of the ordered solvent of the proteins in the solid state according to the hydration level.*

Table 5. Ligands Contained in Crystal Structures Discriminated by PCA Analysis and Ordered Based on Proximity with DES-Containing Crystal Structures

PDB code	ligand	binding site	ref
5v4g	*para*-cymene ruthenium chloride ($C_{10}H_{14}Cl_2Ru$)	CHT1	65
4ng8	cluster of 4 Cs ions	CHT1	66
6f2i	Tb-Xo4 ($C_{20}H_{23}N_5O_4Tb$) and Tb ion	CHT1 and CHT2	67
3ajn	aminomethylamide ($C_2H_6N_2O$)	CHT1	64
3agi	arginine ($C_6H_{15}N_4O_2$)	CHT1 and CHT2	63
4hp0	1-deoxynojrimycin ($C_6H_{13}NO_4$)	CHT1	68
4hpi	1-deoxynojrimycin ($C_6H_{13}NO_4$)	CHT1	68
2hub	formic acid (CH_2O_2) and D-(−)-tartaric acid ($C_4H_6O_6$)	CHT1	69
3ato	ethyl glycinate ($C_4H_9NO_2$)	CHT2	63
6ro3	Re4(mu3-OH)4(CO)12 ($C_{12}O_{16}Re_4$)	CHT2	70
5i4y	urea (CH_4N_2O)	CHT2	61

CONCLUSIONS

Despite the extensive studies that have been dedicated to DESs, their use as solvents to crystallize natural and bioactive molecules is still in its infancy. The presence of water in the intermolecular network of DESs has proven to be critical in making them suitable for crystallization. The present study

https://doi.org/10.1021/acssuschemeng.1c01230
ACS Sustainable Chem. Eng. 2021, 9, 8435−8449

investigates for the first time the effectiveness of different DESs as crystallization media for biological macromolecules, providing an atomic view of the DES supramolecular network. Experimental data show that DESs can indeed serve as useful crystallization media for proteins *when interactions between individual DES components are stronger than those occurring between DESs and the protein residues*. In the presence of moderate-to-strong interactions between DESs and protein, nucleation probability increases with the hydration level (see section Analysis of the Ligands). At the same time, the tunability of physicochemical properties of DES mixtures, by varying the nature of the DES components, discloses countless possibilities of finding the right eutectic mixture for each protein to be crystallized.

Hen-egg-white lysozyme X-ray structures were obtained in three hydrophilic DESs: choline chloride:urea (1:2 mol mol^{-1}), choline chloride:glycerol (1:2 mol mol^{-1}), and choline chloride:glutamic acid (1:2 mol mol^{-1}). Conversely, the hydrophilic DES choline chloride:oxalic acid (1:1 mol mol^{-1}) was found to exalt the interactions between DES components at the expense of those between protein and DES, thereby leading to the precipitation of sodium hydrogen oxalate crystals, independently on the hydration level. In the solid state, strong interactions between individual DES components and protein residues predominate over weaker interactions within DES, as inferred by X-ray diffraction studies when DESs are used in the crystallization cocktail. *Water molecules and chloride/sodium ions interact with the DES constituents, locally modulating the solvent properties and the protein−solvent interactions, thereby strongly impacting the crystallization process, where the nucleation probability increases with the hydration level*. Conversely, crystal lattice properties are weakly affected by the presence of DES that induces negligible perturbations on the overall protein conformation. Long-range interactions among DES components are strongly influenced by crystal packing, as they involve symmetrically equivalent molecules.

According to the crystallographic data of hen-egg-white lysozyme grown in the presence of different DESs and at different hydration levels, it emerges that DESs might play a crucial role for specific applications, such as fragment screening experiments, *in situ* measurements, and room-temperature data collections. In fact, in such cases, the use of DESs could reduce crystal mobility, thereby preserving protein crystals by osmotic shock and radiation damage. Other relevant advantages of using DES as protein crystallization media are related to their ability to reduce the dissolution time of protein crystals, thereby increasing the lifetime of proteins in the solid state under harsh conditions from minutes to hours, or even days, and to modulate the protein conformation in the solid state, possibly increasing the activity of the enzymes in the crystal form. These findings open up new horizons for crystallography and pave the way toward novel biotechnological applications of eutectic mixtures. In fact, although further evidence is needed, they suggest that protein crystals can receive a beneficial stabilization in the presence of DESs, even in a small amount. This would come very handy in all the biotechnological applications in which enzymatic reactions can be performed using crystals as heterogeneous biocatalysts that would deteriorate much faster in the absence of DESs.

■ ASSOCIATED CONTENT

Supporting Information

The Supporting Information is available free of charge at https://pubs.acs.org/doi/10.1021/acssuschemeng.1c01230.

Details on materials used for experiments and on conditions explored in crystallization experiments; images from crystallization experiments on Dypb and HEL4 proteins; electron density map calculated for CHT3 and GLU sites; pictures of all the lysozyme crystal structures determined in this study; details about the crystal structure determination of sodium hydrogen oxalate; estimated number of mutual interactions among DES components; results of structural comparison among the lysozyme crystal structures determined in this study, based on RMSD, PAV, and SASA (the latter with and without considering the presence of ligands in the crystal structure) descriptors and on surface distribution functions; choline molecule modeled in the 4aga crystal structure; and results of structural comparison among of a set of 120 lysozyme crystal structures, performed by using PAV and SASA (this latter without considering the ligands) descriptors (PDF)

■ AUTHOR INFORMATION

Corresponding Authors

Massimo Trotta − *Istituto per i Processi Chimico Fisici, Consiglio Nazionale delle Ricerche, I-70125 Bari, Italy*; Email: massimo.trotta@cnr.it

Vito Capriati − *Dipartimento di Farmacia - Scienze del Farmaco, Università degli Studi di Bari "Aldo Moro", I-70125 Bari, Italy*; orcid.org/0000-0003-4883-7128; Email: vito.capriati@uniba.it

Rocco Caliandro − *Istituto di Cristallografia, Consiglio Nazionale delle Ricerche, I-70126 Bari, Italy*; orcid.org/0000-0002-0368-4925; Email: rocco.caliandro@ic.cnr.it

Authors

Benny Danilo Belviso − *Istituto di Cristallografia, Consiglio Nazionale delle Ricerche, I-70126 Bari, Italy*

Filippo Maria Perna − *Dipartimento di Farmacia - Scienze del Farmaco, Università degli Studi di Bari "Aldo Moro", I-70125 Bari, Italy*

Benedetta Carrozzini − *Istituto di Cristallografia, Consiglio Nazionale delle Ricerche, I-70126 Bari, Italy*

Complete contact information is available at: https://pubs.acs.org/10.1021/acssuschemeng.1c01230

Author Contributions

M.T., V.C., and R.C. conceived the study. The DESs were prepared and characterized by F.M.P. Crystallization experiments were carried out by B.D.B. Structural characterization by X-ray diffraction was carried out by B.D.B., while B.C. and R.C. performed the structural comparison. The manuscript was written by the contribution of all the authors.

Notes

The authors declare no competing financial interest.

■ ACKNOWLEDGMENTS

The authors wish to thank the Diamond Light Source for access to beamline I03 (Proposal No. MX15832-23) and beamline I04 (Proposal No. MX21741-13), which contributed

to the results presented here, L. Pollegioni and E. Rosini for supplying the Dypb protein, FUJIFILM Diosynth Biotechnologies (Billingham, U.K.) for providing the HEL4 protein, and F. Baldassarre for help in collecting single-crystal data from salt crystals. This research has been partially supported by the short-term mobility CNR program. F.M.P. and V.C. also wish to thank the Ministero dell'Università e della Ricerca (MUR) for financially supporting this work, which was carried out under the framework of the national PRIN project "Unlocking Sustainable Technologies Through Nature-inspired Solvents" (NATUREChem) (Grant Number 2017A5HXFC_002).

REFERENCES

(1) Smith, E. L.; Abbott, A. P.; Ryder, K. S. Deep Eutectic Solvents (DESs) and Their Applications. *Chem. Rev.* **2014**, *114*, 11060−11082.
(2) Perna, F. M.; Vitale, P.; Capriati, V. Deep eutectic solvents and their applications as green solvents. *Curr. Opin. Green Sust. Chem.* **2020**, *21*, 27−33.
(3) Hansen, B. B.; Spittle, S.; Chen, B.; Poe, D.; Zhang, Y.; Klein, J. M.; Horton, A.; Adhikari, L.; Zelovich, T.; Doherty, B. W.; Gurkan, B.; Maginn, E. J.; Ragauskas, A.; Dadmun, M.; Zawodzinski, T. A.; Baker, G. A.; Tuckerman, M. E.; Savinell, R. F.; Sangoro, J. R. Deep Eutectic Solvents: A Review of Fundamentals and Applications. *Chem. Rev.* **2021**, *121*, 1232−1285.
(4) Dai, Y.; van Spronsen, J.; Witkamp, G.-J.; Verpoorte, R.; Choi, Y. H. Natural deep eutectic solvents as new potential media for green technology. *Anal. Chim. Acta* **2013**, *766*, 61−68.
(5) García-Álvarez, J.; Hevia, E.; Capriati, V. The Future of Polar Organometallic Chemistry Written in Bio-Based Solvents and Water. *Chem. - Eur. J.* **2018**, *24*, 14854−14863.
(6) Cicco, L.; Salomone, A.; Vitale, P.; Ríos-Lombardía, N.; González-Sabín, J.; García-Álvarez, J.; Perna, F. M.; Capriati, V. Addition of Highly Polarized Organometallic Compounds to *N*-*tert*-Butanesulfinyl Imines in Deep Eutectic Solvents under Air: Preparation of Chiral Amines of Pharmaceutical Interest. *ChemSusChem* **2020**, *13*, 3583−3588.
(7) Dilauro, G.; García, S. M.; Tagarelli, D.; Vitale, P.; Perna, F. M.; Capriati, V. Ligand-Free Bioinspired Suzuki−Miyaura Coupling Reactions using Aryltrifluoroborates as Effective Partners in Deep Eutectic Solvents. *ChemSusChem* **2018**, *11*, 3495−3501.
(8) Shaabani, A.; Hooshmand, S. E.; Afshari, R.; Shaabani, S.; Ghasemi, V.; Atharnezhad, M.; Akbari, M. Direct construction of diverse metallophthalocyanines by manifold substrates in a deep eutectic solvent. *J. Solid State Chem.* **2018**, *258*, 536−542.
(9) Karimi, S.; Shekaari, H.; Halimehjani, A. Z.; Niakan, M. Solvent-Free Production of 5-Hydroxymethylfurfural from Deep Eutectic Substrate Reaction Mixtures over a Magnetically Recoverable Solid Acid Catalyst. *ACS Sustainable Chem. Eng.* **2021**, *9*, 326−336.
(10) Cicco, L.; Dilauro, G.; Perna, F. M.; Vitale, P.; Capriati, V. Advances in deep eutectic solvents and water: applications in metal- and biocatalyzed processes, in the synthesis of APIs, and other biologically active compounds. *Org. Biomol. Chem.* **2021**, *19*, 2558−2577.
(11) Cicco, L.; Ríos-Lombardía, N.; Rodríguez-Álvarez, M. J.; Morís, F.; Perna, F. M.; Capriati, V.; García-Álvarez, J.; González-Sabín, J. Programming cascade reactions interfacing biocatalysis with transition-metal catalysis in Deep Eutectic Solvents as biorenewable reaction media. *Green Chem.* **2018**, *20*, 3468−3475.
(12) Vitale, P.; Lavolpe, F.; Valerio, F.; Di Biase, M.; Perna, F. M.; Messina, E.; Agrimi, G.; Pisano, I.; Capriati, V. Sustainable chemoenzymatic preparation of enantiopure (R)-*β*-hydroxy-1,2,3-triazoles via lactic acid bacteria-mediated bioreduction of aromatic ketones and a heterogeneous "click" cycloaddition reaction in deep eutectic solvents. *React. Chem. Eng.* **2020**, *5*, 859−864.
(13) Millia, L.; Dall'Asta, V.; Ferrara, C.; Berbenni, V.; Quartarone, E.; Perna, F. M.; Capriati, V.; Mustarelli, P. Bio-inspired choline chloride-based deep eutectic solvents as electrolytes for lithium-ion batteries. *Solid State Ionics* **2018**, *323*, 44−48.
(14) Milano, F.; Giotta, L.; Guascito, M. R.; Agostiano, A.; Sblendorio, S.; Valli, L.; Perna, F. M.; Cicco, L.; Trotta, M.; Capriati, V. Functional Enzymes in Nonaqueous Environment: The Case of Photosynthetic Reaction Centers in Deep Eutectic Solvents. *ACS Sustainable Chem. Eng.* **2017**, *5*, 7768−7776.
(15) Boldrini, C. L.; Manfredi, N.; Perna, F. M.; Trifiletti, V.; Capriati, V.; Abbotto, A. Dye-Sensitized Solar Cells that use an Aqueous Choline Chloride-Based Deep Eutectic Solvent as Effective Electrolyte Solution. *Energy Technol.* **2017**, *5*, 345−353.
(16) Gotor-Fernández, V.; Paul, C. E. Deep eutectic solvents for redox biocatalysis. *J. Biotechnol.* **2019**, *293*, 24−35.
(17) El Achkar, T.; Fourmentin, S.; Greige-Gerges, H. Deep eutectic solvents: An overview on their interactions with water and biochemical compounds. *J. Mol. Liq.* **2019**, *288*, 111028.
(18) Torres-Salas, P.; del Monte-Martinez, A.; Cutiño-Avila, B.; Rodriguez-Colinas, B.; Alcalde, M.; Ballesteros, A. O.; Plou, F. J. Immobilized biocatalysts: novel approaches and tools for binding enzymes to supports. *Adv. Mater.* **2011**, *23*, 5275−5282.
(19) Bilal, M.; Zhao, Y.; Noreen, S.; Shah, S. Z. H.; Bharagava, R. N.; Iqbal, H. M. N. Modifying bio-catalytic properties of enzymes for efficient biocatalysis: a review from immobilization strategies viewpoint. *Biocatal. Biotransform.* **2019**, *37*, 159−182.
(20) Di Profio, G.; Polino, M.; Nicoletta, F. P.; Belviso, B. D.; Caliandro, R.; Fontananova, E.; De Filpo, G.; Curcio, E.; Drioli, E. Tailored Hydrogel Membranes for Efficient Protein Crystallization. *Adv. Funct. Mater.* **2014**, *24*, 1582−1590.
(21) Mirabelli, V.; Majidi Salehi, S.; Angiolillo, L.; Belviso, B. D.; Conte, A.; Del Nobile, M. A.; Di Profio, G.; Caliandro, R. Enzyme Crystals and Hydrogel Composite Membranes as New Active Food Packaging Material. *Global Challenges* **2018**, *2*, 1700089.
(22) Majidi Salehi, S.; Manjua, A. C.; Belviso, B. D.; Portugal, C. A. M.; Coelhoso, I. M.; Mirabelli, V.; Fontananova, E.; Caliandro, R.; Crespo, J. G.; Curcio, E.; Di Profio, G. Hydrogel Composite Membranes Incorporating Iron Oxide Nanoparticles as Topographical Designers for Controlled Heteronucleation of Proteins. *Cryst. Growth Des.* **2018**, *18*, 3317−3327.
(23) Pusey, M. L.; Paley, M. S.; Turner, M. B.; Rogers, R. D. Protein crystallization using room temperature ionic liquids. *Cryst. Growth Des.* **2007**, *7*, 787−793.
(24) Hekmat, D.; Hebel, D.; Joswig, S.; Schmidt, M.; Weuster-Botz, D. Advanced protein crystallization using water-soluble ionic liquids as crystallization additives. *Biotechnol. Lett.* **2007**, *29*, 1703−1711.
(25) Ionic Liquid Screen, HR2-214, Hampton Research.
(26) Schroder, C. Proteins in Ionic Liquids: Current Status of Experiments and Simulations. *Top. Curr. Chem.* **2017**, *375*, 25.
(27) Belviso, B. D.; Caliandro, R.; Salehi, S. M.; Di Profio, G.; Caliandro, R. Protein Crystallization in Ionic-Liquid Hydrogel Composite Membranes. *Crystals* **2019**, *9*, 253.
(28) Sanchez-Fernandez, A.; Edler, K. J.; Arnold, T.; Alba Venero, D.; Jackson, A. J. Protein conformation in pure and hydrated deep eutectic solvents. *Phys. Chem. Chem. Phys.* **2017**, *19*, 8667−8670.
(29) Kaur, S.; Kumari, M.; Kashyap, H. K. Microstructure of Deep Eutectic Solvents: Current Understanding and Challenges. *J. Phys. Chem. B* **2020**, *124*, 10601−10616.
(30) Hammond, O. S.; Bowron, D. T.; Edler, K. J. The Effect of Water upon Deep Eutectic Solvent Nanostructure: An Unusual Transition from Ionic Mixture to Aqueous Solution. *Angew. Chem., Int. Ed.* **2017**, *56*, 9782−9785.
(31) Florindo, C.; Oliveira, F. S.; Rebelo, L. P. N.; Fernandes, A. M.; Marrucho, I. M. Insights into the Synthesis and Properties of Deep Eutectic Solvents Based on Cholinium Chloride and Carboxylic Acids. *ACS Sustainable Chem. Eng.* **2014**, *2*, 2416−2425.
(32) Florindo, C.; Branco, L. C.; Marrucho, I. M. Quest for Green-Solvent Design: From Hydrophilic to Hydrophobic (Deep) Eutectic Solvents. *ChemSusChem* **2019**, *12*, 1549−1559.
(33) Abbott, A. P.; Capper, G.; Davies, D. L.; Rasheed, R. K.; Tambyrajah, V. Ionic liquids and their use as solventsWO 02/26701 (A2), 2002.

https://doi.org/10.1021/acssuschemeng.1c01230
ACS Sustainable Chem. Eng. 2021, 9, 8435−8449

(34) Ruß, C.; König, B. Low melting mixtures in organic synthesis – an alternative to ionic liquids? *Green Chem.* **2012**, *14*, 2969–2982.
(35) Roberts, J. N.; Singh, R.; Grigg, J. C.; Murphy, M. E.; Bugg, T. D.; Eltis, L. D. Characterization of dye-decolorizing peroxidases from Rhodococcus jostii RHA1. *Biochemistry* **2011**, *50*, 5108–5119.
(36) Jespers, L.; Schon, O.; James, L. C.; Veprintsev, D.; Winter, G. Crystal structure of HEL4, a soluble human VH antibody domain resistant to aggregation. *J. Mol. Biol.* **2004**, *337*, 893–903.
(37) Kabsch, W. XDS. *Acta Crystallogr., Sect. D: Biol. Crystallogr.* **2010**, *66*, 125–132.
(38) Winn, M. D.; Ballard, C. C.; Cowtan, K. D.; Dodson, E. J.; Emsley, P.; Evans, P. R.; Keegan, R. M.; Krissinel, E. B.; Leslie, A. G.; McCoy, A.; McNicholas, S. J.; Murshudov, G. N.; Pannu, N. S.; Potterton, E. A.; Powell, H. R.; Read, R. J.; Vagin, A.; Wilson, K. S. Overview of the CCP4 suite and current developments. *Acta Crystallogr., Sect. D: Biol. Crystallogr.* **2011**, *67*, 235–242.
(39) Tickle, I. J.; Flensburg, C.; Keller, P.; Paciorek, W.; Sharff, A.; Vonrhein, C.; Bricogne, G. *STARANISO*; Global Phasing Ltd.: Cambridge, U.K., 2018.
(40) Caliandro, R.; Carrozzini, B.; Cascarano, G. L.; Giacovazzo, C.; Mazzone, A.; Siliqi, D. Molecular replacement: the probabilistic approach of the program REMO09 and its applications. *Acta Crystallogr., Sect. A: Found. Crystallogr.* **2009**, *65*, 512–527.
(41) Burla, M. C.; Caliandro, R.; Camalli, M.; Carrozzini, B.; Cascarano, G. L.; De Caro, L.; Giacovazzo, C.; Polidori, G.; Siliqi, D.; Spagna, R. IL MILIONE: A suite of computer programs for crystal structure solution of proteins. *J. Appl. Crystallogr.* **2007**, *40*, 609–613.
(42) Petruk, A. A.; Vergara, A.; Marasco, D.; Bikiel, D.; Doctorovich, F.; Estrin, D. A.; Merlino, A. Interaction between Proteins and Ir Based CO Releasing Molecules: Mechanism of Adduct Formation and CO Release. *Inorg. Chem.* **2014**, *53*, 10456–10462.
(43) Terwilliger, T. C.; Grosse-Kunstleve, R. W.; Afonine, P. V.; Moriarty, N. W.; Zwart, P. H.; Hung, L. W.; Read, R. J.; Adams, P. D. Iterative model building, structure refinement and density modification with the PHENIX AutoBuild wizard. *Acta Crystallogr., Sect. D: Biol. Crystallogr.* **2008**, *64*, 61–69.
(44) Adams, P. D.; Afonine, P. V.; Bunkoczi, G.; Chen, V. B.; Davis, I. W.; Echols, N.; Headd, J. J.; Hung, L. W.; Kapral, G. J.; Grosse-Kunstleve, R. W.; McCoy, A. J.; Moriarty, N. W.; Oeffner, R.; Read, R. J.; Richardson, D. C.; Richardson, J. S.; Terwilliger, T. C.; Zwart, P. H. PHENIX: a comprehensive Python-based system for macromolecular structure solution. *Acta Crystallogr., Sect. D: Biol. Crystallogr.* **2010**, *66*, 213–221.
(45) Afonine, P. V.; Grosse-Kunstleve, R. W.; Echols, N.; Headd, J. J.; Moriarty, N. W.; Mustyakimov, M.; Terwilliger, T. C.; Urzhumtsev, A.; Zwart, P. H.; Adams, P. D. Towards automated crystallographic structure refinement with phenix.refine. *Acta Crystallogr., Sect. D: Biol. Crystallogr.* **2012**, *68*, 352–367.
(46) Liebschner, D.; Afonine, P. V.; Moriarty, N. W.; Poon, B. K.; Sobolev, O. V.; Terwilliger, T. C.; Adams, P. D. Polder maps: improving OMIT maps by excluding bulk solvent. *Acta Crystallogr. D. Biol. Crystallogr.* **2017**, *73*, 148–157.
(47) Chen, V. B.; Arendall, W. B.; Headd, J. J.; Keedy, D. A.; Immormino, R. M.; Kapral, G. J.; Murray, L. W.; Richardson, J. S.; Richardson, D. C. MolProbity: all-atom structure validation for macromolecular crystallography. *Acta Crystallogr., Sect. D: Biol. Crystallogr.* **2010**, *66*, 12–21.
(48) Vaguine, A. A.; Richelle, J.; Wodak, S. J. SFCHECK: a unified set of procedures for evaluating the quality of macromolecular structure-factor data and their agreement with the atomic model. *Acta Crystallogr., Sect. D: Biol. Crystallogr.* **1999**, *55*, 191–205.
(49) Humphrey, W.; Dalke, A.; Schulten, K. VMD: Visual molecular dynamics. *J. Mol. Graphics* **1996**, *14*, 33–38.
(50) Caliandro, R.; Rossetti, G.; Carloni, P. Local fluctuations and conformational transitions in proteins. *J. Chem. Theory Comput.* **2012**, *8*, 4775–4785.
(51) Liuzzi, V. C.; Mirabelli, V.; Cimmarusti, M. T.; Haidukowski, M.; Leslie, J. F.; Logrieco, A. F.; Caliandro, R.; Fanelli, F.; Mulè, G. Enniatin and beauvericin biosynthesis in Fusarium species: Production profiles and structural determinant prediction. *Toxins* **2017**, *9*, 45.
(52) Caliandro, R.; Belviso, B. D. RootProf: Software for multivariate analysis of unidimensional profiles. *J. Appl. Crystallogr.* **2014**, *47*, 1087–1096.
(53) Krissinel, E.; Henrick, K. Secondary-structure matching (SSM), a new tool for fast protein structure alignment in three dimensions. *Acta Crystallogr., Sect. D: Biol. Crystallogr.* **2004**, *60*, 2256–2268.
(54) Chen, X.; Weber, I.; Harrison, R. W. Hydration Water and Bulk Water in Proteins Have Distinct Properties in Radial Distributions Calculated from 105 Atomic Resolution Crystal Structures. *J. Phys. Chem. B* **2008**, *112*, 12073–12080.
(55) *The PyMOL Molecular Graphics System*, Version 1.8.4.0 Open-Source; (Copyright (C) 2003–2021); Schrödinger, LLC.
(56) Cruickshank, D. Remarks about protein structure precision. *Acta Crystallogr., Sect. D: Biol. Crystallogr.* **1999**, *55*, 583–601.
(57) Kumari, P.; Kumari, M.; Kashyap, H. K. How Pure and Hydrated Reline Deep Eutectic Solvents Affect the Conformation and Stability of Lysozyme: Insights from Atomistic Molecular Dynamics Simulations. *J. Phys. Chem. B* **2020**, *124*, 11919–11927.
(58) Gabriele, F.; Chiarini, M.; Germani, R.; Tiecco, M.; Spreti, N. Effect of water addition on choline chloride/glycol deep eutectic solvents: characterization of their structural and physicochemical properties. *J. Mol. Liq.* **2019**, *291*, 111301.
(59) Hagemans, D.; van Belzen, I. A. E. M.; Morán Luengo, T.; Rüdiger, S. G. D. A script to highlight hydrophobicity and charge on protein surfaces. *Front. Mol. Biosci.* **2015**, *2*, 56.
(60) Kowacz, M.; Mukhopadhyay, A.; Carvalho, A. L.; Esperanca, J. M. S. S.; Romao, M. J.; Rebelo, L. P. N. Hofmeister Effects of Ionic Liquids in Protein Crystallization: Direct and Water-Mediated Interactions. *CrystEngComm* **2012**, *14*, 4912–4921.
(61) Raskar, T.; Khavnekar, S.; Hosur, M. Time-dependent X-ray diffraction studies on urea/hen egg white lysozyme complexes reveal structural changes that indicate onset of denaturation. *Sci. Rep.* **2016**, *6*, 32277.
(62) Salem, M.; Mauguen, Y.; Prangé, T. On the edge of the denaturation process: Application of X-ray diffraction to barnase and lysozyme cross-linked crystals with denaturants in molar concentrations. *Biochim. Biophys. Acta, Proteins Proteomics* **2006**, *1764*, 903–912.
(63) Ito, L.; Shiraki, K.; Matsuura, T.; Okumura, M.; Hasegawa, K.; Baba, S.; Yamaguchi, H.; Kumasaka, T. High-resolution X-ray analysis reveals binding of arginine to aromatic residues of lysozyme surface: implication of suppression of protein aggregation by arginine. *Protein Eng., Des. Sel.* **2011**, *24*, 269–274.
(64) Ito, L.; Shiraki, K.; Makino, M.; Hasegawa, K.; Kumasaka, T. Glycine amide shielding on the aromatic surfaces of lysozyme: Implication for suppression of protein aggregation. *FEBS Lett.* **2011**, *585*, 555–560.
(65) Sullivan, M. P.; Groessl, M.; Meier, S. M.; Kingston, R. L.; Goldstone, D. C.; Hartinger, C. G. The metalation of hen egg white lysozyme impacts protein stability as shown by ion mobility mass spectrometry, differential scanning calorimetry, and X-ray crystallography. *Chem. Commun.* **2017**, *53*, 4246–4249.
(66) Benas, P.; Auzeil, N.; Legrand, L.; Brachet, F.; Regazzetti, A.; RIes-Kautt, M. Weak protein-cationic co-ion interactions addressed by X-ray crystallography and mass spectrometry. *Acta Crystallogr., Sect. D: Biol. Crystallogr.* **2014**, *70*, 2217–2231.
(67) Engilberge, S.; Riobe, F.; Wagner, T.; Di Pietro, S.; Breyton, C.; Franzetti, B.; Shima, S.; Girard, E.; Dumont, E.; Maury, O. Unveiling the binding modes of the crystallophor, a Terbium-based nucleating and phasing molecular agent for protein Crystallography. *Chem. - Eur. J.* **2018**, *24*, 9739–9746.
(68) Ogata, M.; Umemoto, N.; Ohnuma, T.; Numata, T.; Suzuki, A.; Usui, T.; Fukamizo, T. A novel transition-state analogue for lysozyme, 4-O-beta-tri-N-acetylchitotriosyl moranoline, provided evidence supporting the covalent glycosyl-enzyme intermediate. *J. Biol. Chem.* **2013**, *288*, 6072–6082.

https://doi.org/10.1021/acssuschemeng.1c01230
ACS Sustainable Chem. Eng. 2021, 9, 8435–8449

(69) Kumar, E. K.; Prabhu, N. P. Differential effects of ionic and non-ionic surfactants on lysozyme fibrillation. *Phys. Chem. Chem. Phys.* **2014**, *16*, 24076−24088.
(70) Brink, A.; Helliwell, J. R. Formation of a highly dense tetrarhenium cluster in a protein crystal and its implications in medical imaging. *IUCrJ* **2019**, *6*, 695−702.

https://doi.org/10.1021/acssuschemeng.1c01230
ACS Sustainable Chem. Eng. 2021, 9, 8435−8449